The Astrophysical Journal Letters, 931:L7 (8pp), 2022 May 20 https://doi.org/10.3847/2041-8213/ac63b0

Looking at the Distant Universe with the MeerKAT Array: Discovery of a Luminous OH Megamaser at $z > 0.5$

Marcin Glowacki[1,2,3], Jordan D. Collier[1,4,5,6], Amir Kazemi-Moridani[7], Bradley Frank[1,4,8], Hayley Roberts[9], Jeremy Darling[9], Hans-Rainer Klöckner[10], Nathan Adams[11,12], Andrew J. Baker[2,7], Matthew Bershady[4,13,14], Tariq Blecher[15], Sarah-Louise Blyth[4], Rebecca Bowler[11,12], Barbara Catinella[16,17], Laurent Chemin[18], Steven M. Crawford[19], Catherine Cress[2], Romeel Davé[2,20], Roger Deane[21,22], Erwin de Blok[4,23,24], Jacinta Delhaize[4], Kenneth Duncan[20], Ed Elson[2], Sean February[8], Eric Gawiser[7], Peter Hatfield[11], Julia Healy[23], Patricia Henning[25,26], Kelley M. Hess[23,24,27], Ian Heywood[8,11,15], Benne W. Holwerda[28], Munira Hoosain[4], John P. Hughes[7], Zackary L. Hutchens[29], Matt Jarvis[2,11], Sheila Kannappan[29], Neal Katz[30], Dušan Kereš[31], Marie Korsaga[32,33], Renée C. Kraan-Korteweg[4], Philip Lah[34], Michelle Lochner[2,8], Natasha Maddox[35], Sphesihle Makhathini[21], Gerhardt R. Meurer[16], Martin Meyer[16], Danail Obreschkow[16], Se-Heon Oh[36], Tom Oosterloo[23,24], Joshua Oppor[13], Hengxing Pan[2,11], D. J. Pisano[37,38], Nandrianina Randriamiarinarivo[2], Swara Ravindranath[39], Anja C. Schröder[40], Rosalind Skelton[14], Oleg Smirnov[8,15], Mathew Smith[41,42], Rachel S. Somerville[43], Raghunathan Srianand[44], Lister Staveley-Smith[16,17], Masayuki Tanaka[45,46], Mattia Vaccari[1,2,47], Wim van Driel[48], Marc Verheijen[49], Fabian Walter[50], John F. Wu[39], and Martin A. Zwaan[51]

[1] Inter-University Institute for Data Intensive Astronomy (IDIA), South Africa
[2] Department of Physics and Astronomy, University of the Western Cape, Robert Sobukwe Road, Bellville 7535, South Africa
[3] International Centre for Radio Astronomy Research (ICRAR), Curtin University, Bentley, WA 6102, Australia; marcin.glowacki@curtin.edu.au
[4] Department of Astronomy, University of Cape Town, Private Bag X3, Rondebosch 7700, South Africa
[5] School of Science, Western Sydney University, Locked Bag 1797, Penrith, NSW 2751, Australia
[6] CSIRO Astronomy and Space Science, P.O. Box 1130, Bentley, WA 6102, Australia
[7] Department of Physics and Astronomy, Rutgers, the State University of New Jersey, 136 Frelinghuysen Road, Piscataway, NJ 08854-8019, USA
[8] South African Radio Astronomy Observatory, 2 Fir Street, Black River Park, Observatory, 7925, South Africa
[9] Center for Astrophysics and Space Astronomy, Department of Astrophysical and Planetary Sciences, University of Colorado, 389 UCB, Boulder, CO 80309-0389, USA
[10] Max-Planck-Institut für Radioastronomie, Auf dem Hügel 69, D-53121, Bonn, Germany
[11] Astrophysics, University of Oxford, Denys Wilkinson Building, Keble Road, Oxford OX1 3RH, UK
[12] Jodrell Bank Centre for Astrophysics, School of Physics and Astronomy, University of Manchester, Manchester M13 9PL, UK
[13] Department of Astronomy, University of Wisconsin-Madison, 475 N. Charter Street, Madison, WI 53706, USA
[14] South African Astronomical Observatory, P.O. Box 9, Observatory 7935, South Africa
[15] Department of Physics and Electronics, Rhodes University, P.O. Box 94, Makhanda (Grahamstown), 6140, South Africa
[16] International Centre for Radio Astronomy Research (ICRAR), The University of Western Australia, 35 Stirling Highway, Perth, WA 6009, Australia
[17] ARC Centre of Excellence for All Sky Astrophysics in 3 Dimensions (ASTRO 3D), Australia
[18] Centro de Astronomia—CITEVA, Universidad de Antofagasta, Avenida Angamos 601, Antofagasta 1270300, Chile
[19] unaffiliated
[20] Institute for Astronomy, University of Edinburgh, Royal Observatory, Blackford Hill, Edinburgh, EH9 3HJ, UK
[21] Wits Centre for Astrophysics, School of Physics, University of the Witwatersrand, 1 Jan Smuts Avenue 2000, South Africa
[22] Department of Physics, University of Pretoria, Private Bag X20, Pretoria 0028, South Africa
[23] ASTRON, the Netherlands Institute for Radio Astronomy, Oude Hoogeveensedijk 4, 7991 PD, Dwingeloo, The Netherlands
[24] Kapteyn Astronomical Institute, University of Groningen, P.O. Box 800, 9700 AV Groningen, The Netherlands
[25] National Radio Astronomy Observatory, Pete V. Domenici Science Operations Center, P.O. Box O, 1003 Lopezville Road, Socorro, NM 87801-0387, USA
[26] Department of Physics and Astronomy, University of New Mexico, 210 Yale Boulevard NE, Albuquerque, NM 87106, USA
[27] Instituto de Astrofísica de Andalucía (CSIC), Glorieta de la Astronomía s/n, E-18008 Granada, Spain
[28] Department of Physics and Astronomy, 102 Natural Science Building, University of Louisville, Louisville, KY 40292, USA
[29] Department of Physics & Astronomy, CB3255, University of North Carolina, Chapel Hill, NC 27516, USA
[30] Department of Astronomy, University of Massachusetts, Amherst, MA 01003, USA
[31] Center for Astrophysics and Space Sciences, University of California San Diego, 9500 Gilman Drive, La Jolla, CA 92093, USA
[32] Université de Strasbourg, CNRS, Observatoire astronomique de Strasbourg, UMR 7550, F-67000 Strasbourg, France
[33] Laboratoire de Physique et de Chimie de l'Environnement, Observatoire d'Astrophysique de l'Université Joseph Ki-Zerbo (ODAUO), 03 BP 7021, Ouaga 03, Burkina Faso
[34] Research School of Astronomy and Astrophysics, Australian National University, Canberra, ACT 2611, Australia
[35] University Observatory, Faculty of Physics, Ludwig-Maximilians-Universität, Scheinerstr. 1, D-81679 Munich, Germany
[36] Department of Physics and Astronomy, Sejong University, 209 Neungdong-ro, Gwangjin-gu, Seoul, Republic of Korea
[37] Department of Physics & Astronomy, West Virginia University, Morgantown, WV 26506, USA
[38] Gravitational Wave and Cosmology Center, Chestnut Ridge Research Building, Morgantown, WV 26505, USA
[39] Space Telescope Science Institute, 3700 San Martin Drive, Baltimore, MD 21218-2410, USA
[40] Max-Planck-Institut für extraterrestrische Physik, Giessenbachstraße 1, D-85748 Garching bei München, Germany
[41] School of Physics and Astronomy, University of Southampton, Southampton, SO17 1BJ, UK
[42] Univ Lyon, Univ Claude Bernard Lyon 1, CNRS, IP2I Lyon / IN2P3, IMR 5822, F-69622, Villeurbanne, France
[43] Center for Computational Astrophysics, Flatiron Institute, New York, NY 10010, USA
[44] IUCAA, Postbag 4, Ganeshkhind, Pune 411007, India
[45] Department of Astronomical Science, The Graduate University for Advanced Studies, SOKENDAI, 2-21-1 Osawa, Mitaka, Tokyo, 181-8588, Japan
[46] National Astronomical Observatory of Japan, 2-21-1 Osawa, Mitaka, Tokyo, 181-8588, Japan
[47] INAF—Istituto di Radioastronomia, via Gobetti 101, I-40129 Bologna, Italy
[48] GEPI, Observatoire de Paris, PSL Université, CNRS UMR 8111, 5 place Jules Janssen, F-92190 Meudon, France
[49] Kapteyn Astronomical Institute, University of Groningen, Landleven 12, 9747 AD, Groningen, The Netherlands
[50] Max-Planck-Institut für Astronomie (MPIA), Königstuhl 16, D-69117 Heidelberg, Germany

[51] European Southern Observatory, Karl-Schwarzschild-Strasse 2, D-85748 Garching, Germany
Received 2022 February 10; revised 2022 March 29; accepted 2022 March 29; published 2022 May 19

Abstract

In the local universe, OH megamasers (OHMs) are detected almost exclusively in infrared-luminous galaxies, with a prevalence that increases with IR luminosity, suggesting that they trace gas-rich galaxy mergers. Given the proximity of the rest frequencies of OH and the hyperfine transition of neutral atomic hydrogen (H I), radio surveys to probe the cosmic evolution of H I in galaxies also offer exciting prospects for exploiting OHMs to probe the cosmic history of gas-rich mergers. Using observations for the Looking At the Distant Universe with the MeerKAT Array (LADUMA) deep H I survey, we report the first untargeted detection of an OHM at $z > 0.5$, LADUMA J033046.20−275518.1 (nicknamed "Nkalakatha"). The host system, WISEA J033046.26−275518.3, is an infrared-luminous radio galaxy whose optical redshift $z \approx 0.52$ confirms the MeerKAT emission-line detection as OH at a redshift $z_{\rm OH} = 0.5225 \pm 0.0001$ rather than H I at lower redshift. The detected spectral line has 18.4σ peak significance, a width of $459 \pm 59\,{\rm km\,s^{-1}}$, and an integrated luminosity of $(6.31 \pm 0.18\,[\text{statistical}] \pm 0.31\,[\text{systematic}]) \times 10^3\,L_\odot$, placing it among the most luminous OHMs known. The galaxy's far-infrared luminosity $L_{\rm FIR} = (1.576 \pm 0.013) \times 10^{12}\,L_\odot$ marks it as an ultraluminous infrared galaxy; its ratio of OH and infrared luminosities is similar to those for lower-redshift OHMs. A comparison between optical and OH redshifts offers a slight indication of an OH outflow. This detection represents the first step toward a systematic exploitation of OHMs as a tracer of galaxy growth at high redshifts.

Unified Astronomy Thesaurus concepts: Megamasers (1023); Hydroxyl masers (771); Radio loud quasars (1349); Galaxy mergers (608); Starburst galaxies (1570); Ultraluminous infrared galaxies (1735)

1. Introduction

OH megamasers (OHMs) are luminous 18 cm wavelength masers, produced in the centers of luminous and ultraluminous infrared galaxies (LIRGs and ULIRGs) that have undergone merger-induced starburst activity (Lo 2005), rich in dense gas (Darling 2007), and in some cases host luminous active galactic nuclei (AGNs; Klöckner et al. 2003). Four 18 cm lines connect the four hyperfine levels within the $^2\Pi_{3/2}(J = 3/2)$ ground state of the OH molecule: two main lines at 1665 and 1667 MHz, and two satellite lines at 1612 and 1720 MHz. In contrast to Galactic OH masers, extragalactic OHMs have large line widths and main line flux ratios $F_{1667}/F_{1665} > 1$. These attributes, along with the weakness of their satellite lines (McBride et al. 2013), can be naturally explained by a model in which OHMs are powered by radiative pumping through 53 μm lines that overlap in velocity and in which different projected distributions of masing clumps can account for observations of both diffuse and compact emitting structures (Lockett & Elitzur 2008).

The most extensive OHM survey in the local universe has been conducted with Arecibo, with a focus on the detection of $z > 0.1$ systems (Darling & Giovanelli 2002a). In total, 53 OHMs were detected, spanning the redshift range $0.10 \leqslant z \leqslant 0.27$. Although Combes et al. (2021) report a tentative 3σ detection of the 1720 MHz satellite line in emission in a targeted MeerKAT observation of the $z = 0.89$ quasar PKS 1830−211, the main lines of OH have not been detected in emission at $z > 0.27$ up to now.

The local demographics of OHMs have been used to predict their occurrence at higher redshifts, where they are likely to represent a significant source of contamination for H I surveys (Briggs 1998; Darling & Giovanelli 2002b; Suess et al. 2016; Roberts et al. 2021). Such surveys will be conducted by the interferometers that include the Square Kilometre Array (SKA) and its pathfinder facilities, such as MeerKAT (Jonas & MeerKAT Team 2016) and the Australian SKA Pathfinder (ASKAP; DeBoer et al. 2009). Although ULIRGs are more prevalent at higher redshifts (Takeuchi et al. 2005), in part because normal star-forming galaxies at earlier epochs are likely to have $L_{\rm FIR} > 10^{12}\,L_\odot$ even in the absence of recent merging (e.g., Reddy et al. 2008), OHMs have the potential to provide new constraints on the cosmic history of gas-rich mergers.

We report the first untargeted detection of an OHM at $z > 0.27$ from early observations for the Looking At the Distant Universe with the MeerKAT Array (LADUMA; Blyth et al. 2016) deep H I survey. Section 2 describes the acquisition and processing of the MeerKAT data in which the OH line was detected, and Section 3 presents our measurements and interpretation of the line parameters. In Section 4, we discuss the implications of this OHM in the context of previous knowledge of OHM hosts at lower redshifts and future observations probing higher redshifts; Section 5 summarizes our conclusions. The paper assumes a flat ΛCDM cosmology with $\Omega_m = 0.3$, $\Omega_\Lambda = 0.7$, and $H_0 = 73.3\,{\rm km\,s^{-1}\,Mpc^{-1}}$ (Wong et al. 2020).

2. Observations

2.1. MeerKAT

MeerKAT is a fixed-configuration array of 64 antennas equipped with receivers spanning the L (900–1670 MHz) and UHF (580–1015 MHz) bands. These overlapping frequency ranges access redshift ranges of $0 \leqslant z_{\rm H\,I} \leqslant 0.58$ and $0.40 \leqslant z_{\rm H\,I} \leqslant 1.45$ for the H I line and $0 \leqslant z_{\rm OH} \leqslant 0.85$ and $0.64 \leqslant z_{\rm OH} \leqslant 1.87$, adopting the stronger of the two main OH lines (at a rest frequency of 1667.359 MHz) to define $z_{\rm OH}$. The LADUMA deep H I survey is using both L and UHF bands to probe the evolution of gas in galaxies over cosmic time. LADUMA is targeting a single pointing on the sky (03:32:30.4 −28:07:57 J2000) that encompasses the extended Chandra Deep Field South (ECDFS) and lies roughly at the center of near-IR imaging coverage from the VISTA Deep Extragalactic

Observations (VIDEO) survey (Jarvis et al. 2013). Because the solid angle of MeerKAT's primary beam is inversely proportional to the square of the observing frequency, the cosmic volume LADUMA probes for any single spectral line expands with redshift like a trumpet (e.g., a South African vuvuzela). Across the L band in particular, MeerKAT's circular field of view increases (at the half-power level) from 0.7 deg^2 at 1667 MHz to 0.9 deg^2 at 1420.4 MHz to 2.3 deg^2 at 900 MHz.

The first official L-band survey observation for LADUMA that used the 32k mode of the MeerKAT correlator (featuring 32,768 channels, each of width 26.1 kHz) was taken on 2019 December 12 with 58 of the 64 antennas in operation. The bright radio galaxy PKS 1934–63 was used as a flux and bandpass calibrator (observed for 10 minutes); the nearby quasar PKS 0237–233 was observed as a gain calibrator for 3.5 minutes after each 20-minute observation of the LADUMA field. The total on-source integration time was 7.3 hr.

We reduced the data across the full L band, excluding regions affected by radio frequency interference (RFI), after splitting into 25 MHz spectral windows (SPWs). For the source discussed in this paper, the relevant SPW spans 1086–1111 MHz. Bandpass, flux, and phase calibration were performed using the PROCESS-MEERKAT pipeline,[52] which is written in Python, uses a purpose-built CASA (McMullin et al. 2007) Singularity container, and employs MPICASA (a parallelized form of CASA). Flux calibration used the Reynolds (1994) model for the spectrum of PKS 1934−63, which is ultimately tied to northern hemisphere calibrators with flux uncertainties of ∼5% at ∼1 GHz (e.g., Perley & Butler 2017). The CASA task tclean was used with robust = 0 to create an initial continuum model as a basis for phase and amplitude self-calibration, after which model continuum visibility data were subtracted from the corrected visibility data using the CASA task uvsub. A third-order polynomial fit to the continuum was then calculated and subtracted using the CASA task uvcontsub for all channels in each SPW to remove residual continuum emission from the spectral line data. Finally, spectral line cubes were created using tclean with robust = 0.5 and no cleaning; all channels in the resulting (dirty) cubes were convolved to a common synthesized beam of $14\farcs2 \times 12\farcs2$ at a position angle of $-15\fdg8$. The rms per 26.1 kHz channel was found to increase with frequency across the 1086–1111 MHz SPW, with a value of 0.40 mJy beam^{-1} near 1095 MHz. All data were reduced on the ilifu cloud computing facility.[53]

Visual inspection of the continuum-subtracted 26.1 kHz channel data cube with the Cube Analysis and Rendering Tool for Astronomy (CARTA; Comrie et al. 2020) revealed a bright spectral line at an observed frequency of 1095 MHz, which we designate as LADUMA J033046.20−275518.1 and describe in detail in Section 3.1.

2.2. Archival Data

LADUMA J033046.20−275518.1 has a clear galaxy counterpart in WISE imaging (WISEA J033046.26–275518.3) and in previous radio continuum mapping by the Australia Telescope Large Area Survey (Mao et al. 2012; Franzen et al. 2015). The galaxy has a bent-tail radio morphology (Dehghan et al. 2014) and has been classified as a narrow-angle (or head–tail) radio galaxy (that is, the bent radio structure lies on one side of the optical host galaxy). The source has also been detected in dust emission by the Multiband Imaging Photometer for Spitzer (MIPS; Rieke et al. 2004) on the Spitzer Space Telescope (Hanish et al. 2015) and by the Spectral and Photometric Imaging Receiver (SPIRE; Griffin et al. 2010) on the Herschel Space Observatory (Oliver et al. 2012; Shirley et al. 2021). Table 1 lists selected photometry for the source in the infrared and radio. Optical spectroscopy has yielded two independent redshift measurements of $z = 0.5245$ (Eales et al. 2009) and $z = 0.5247$ (Mao et al. 2012), neither with a quoted uncertainty; in this paper, we average these two measurements and adopt the ∼100 km s^{-1} uncertainty that is typical for AAT redshifts of similar vintage (see, e.g., Section 1 of Baldry et al. 2014), yielding $z_{\rm opt} = 0.5246 \pm 0.0005$.

Table 1
Selected Photometry for LADUMA J033046.20−275518.1

Source	Observed Wavelength	Flux Density	References
WISE	3.4 μm	0.122 ± 0.005 mJy	Wright et al. (2010)
WISE	4.6 μm	0.084 ± 0.007 mJy	Wright et al. (2010)
WISE	12 μm	0.928 ± 0.085 mJy	Wright et al. (2010)
Spitzer/MIPS	70 μm	141.11 ± 0.66 mJy[a]	Hanish et al. (2015)
Spitzer/MIPS	160 μm	208.34 ± 2.13 mJy[a]	Hanish et al. (2015)
Herschel/SPIRE	250 μm	90.93 ± 0.65 mJy	Shirley et al. (2021)
Herschel/SPIRE	350 μm	42.36 ± 1.53 mJy	Shirley et al. (2021)
Herschel/SPIRE	500 μm	17.6 ± 3.7 mJy	Shirley et al. (2021)
ATCA	20 cm	0.42 ± 0.029 mJy	Franzen et al. (2015)

Note.
[a] Flux density extracted from a point-spread function (PSF) fit.

We can determine the host galaxy's infrared luminosity using the source redshift and far-infrared photometry. By fitting emissivity-weighted blackbody functions to 1000 realizations of the Spitzer/MIPS and Herschel/SPIRE flux densities between 70 and 350 μm (sampling their respective uncertainties), we derive a rest-frame dust temperature $T_d = 41.9 \pm 0.6$ K, a dust emissivity index $\beta = 1.67 \pm 0.06$ (for $\tau_\nu \propto \nu^\beta$), and a far-IR (rest-frame 42.5–122.5 μm) flux $(6.30 \pm 0.05) \times 10^{-12}$ erg s^{-1} cm^{-2}. Using the cosmology adopted for this paper and the redshift measured in Section 3.1 below, we then arrive at $L_{\rm FIR} = (1.576 \pm 0.013) \times 10^{12}\,L_\odot$, confirming the source as a ULIRG as previously noted by Moncelsi et al. (2011).

3. Results

3.1. OH Emission Properties

The spatial centroid of LADUMA J033046.20–275518.1 lies at R.A. 03:30:46.20 and decl. −27:55:18.17 (J2000) with uncertainties of $\pm 0\farcs7$ (calculated as beam size divided by the signal-to-noise ratio S/N)—consistent with the centroids determined for its counterparts at other wavelengths, within their own uncertainties of $\sim 0\farcs5$ or greater. At this position and the observed line frequency, the primary beam correction was a factor $\sim (0.72)^{-1}$, which we applied using CASA before measuring line parameters.

In the right panel of Figure 1, we show the spectrum integrated over a 15″ aperture, with frequency Doppler-

[52] https://idia-pipelines.github.io/docs/processMeerKAT
[53] https://docs.ilifu.ac.za/#/about/what_is

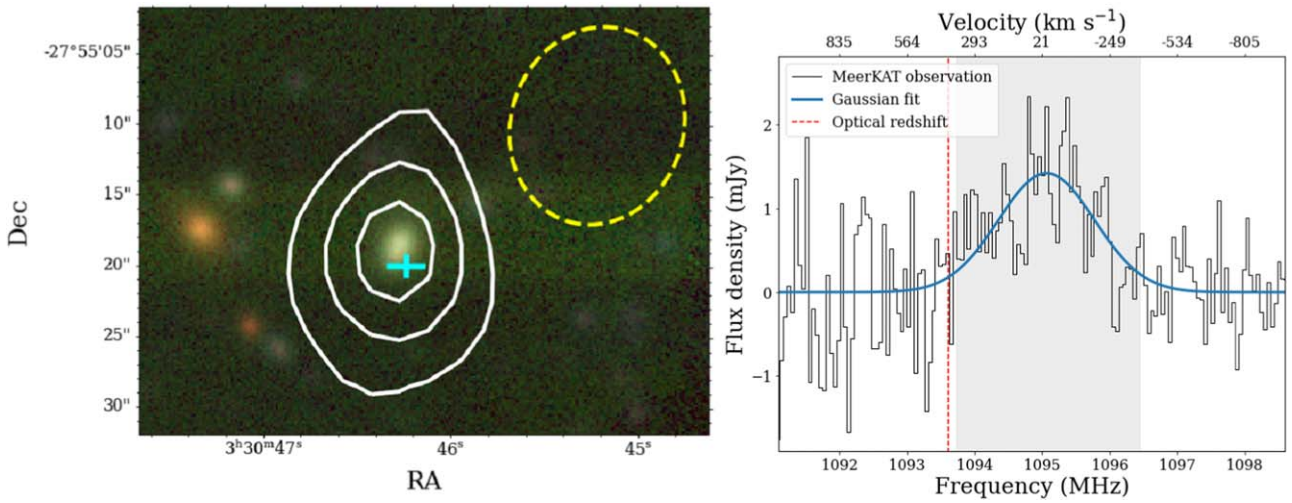

Figure 1. Left: RGB composite image made from the *grz* filters of archival Hyper Suprime-Cam (HSC) data. White contours are from the zeroth-moment map of our MeerKAT observation with no masking applied, integrated across ∼600 km s^{-1}, at multiples of 5σ (1σ = 0.0295 Jy beam^{-1} km s^{-1}). The cyan cross indicates the centroid position and uncertainties from the Franzen et al. (2015) observation with ATCA. The 14.″2 × 12.″2 MeerKAT synthesized beam is plotted as a dashed yellow ellipse. Right: spectrum of the detected OHM, with frequency Doppler-corrected to a heliocentric reference frame and rebinned from its native 26.1 kHz resolution by a factor of 2. The rest-frame velocity range included in the moment map is shaded gray; the best Gaussian fit to the OH emission profile is overlaid in blue. The red dashed line indicates the frequency (1093.7 MHz) where the 1667 MHz line would have appeared for $z_{\rm OH} = z_{\rm opt}$; that $z_{\rm OH} < z_{\rm opt}$ suggests a possible OH outflow.

corrected to the heliocentric reference frame and rebinned by a factor of 2. At the observed frequency, each rebinned (52.2 kHz) channel corresponds to 14.3 km s^{-1} in rest-frame velocity. A single-Gaussian fit to the line spectrum yields (with fit uncertainties noted as errors) a central frequency of $\nu = 1095.07 \pm 0.09$ MHz, a rest-frame line width $\Delta v = 459 \pm 59$ km s^{-1} (FWHM, which corresponds to an observed frequency width of 1.68 MHz), a peak flux density of 1.42 ± 0.16 [$\pm$0.07] mJy,[54] and a total spectral line flux $F_{\rm line} = 0.69 \pm 0.02$ [$\pm$0.03] Jy km s^{-1} that agrees well with a direct integral of the spectrum (0.69 ± 0.02 [$\pm$0.03] Jy km s^{-1}).

We note that the 1665 MHz OH line may contribute to the measured line flux and width, although this fainter feature is not yet detected in this single-track observation nor currently preferred over a single-Gaussian fit. Given the presence of a multiwavelength counterpart with a previously measured optical redshift $z = 0.5246$, it is clear that our detection is hydroxyl emission at $z_{\rm OH} = 0.5225 \pm 0.0001$ (identified as the 1667.359 MHz transition) rather than H I emission at $z_{\rm H\,I} = 0.2970$. From the integrated line flux, we use the general relation for spectral line luminosity

$$\frac{L_{\rm line}}{L_\odot} = 1.0234 \left(\frac{\nu}{\rm MHz}\right)\left(\frac{F_{\rm line}}{\rm Jy\ km\ s^{-1}}\right)\left(\frac{D_L}{\rm Gpc}\right)^2 \quad (1)$$

in terms of observed frequency $\nu = 1095.1 \pm 0.1$ MHz and luminosity distance $D_L = 2.85 \pm 0.02$ Gpc for our adopted cosmology, obtaining an equivalent isotropic luminosity of $L_{\rm OH} = (6.31 \pm 0.18\ [\pm 0.31]) \times 10^3\, L_\odot$.

The left panel of Figure 1 shows contours from the zeroth-moment map for the source, integrated over 600 km s^{-1} and overlaid on a composite image made from the *grz* filters of archival Hyper Suprime-Cam (HSC; Miyazaki et al. 2018) data. The cyan cross indicates the ATCA position and its uncertainties from Franzen et al. (2015), and the yellow ellipse shows the MeerKAT synthesized beam. The OH emission is spatially unresolved, with S/N ∼ 18.4 relative to the rms in the zeroth-moment map away from the source. Figure 2 shows the velocity channel maps of the source after rebinning by an additional factor of 4 to a rest-frame velocity resolution of 57.2 km s^{-1}.

3.2. Confirmation of the 1667 MHz Identification

Notwithstanding the good agreement with a previously measured optical redshift, we have considered whether the detected emission could correspond to a weaker OH line (e.g., the 1612 or 1720 MHz satellite line, which can exhibit conjugate behavior; Darling 2004) rather than the main 1667 MHz transition. In this scenario, we would expect an additional detection of the (brighter) 1667 MHz main line at a different frequency (1132.5 or 1061.2 MHz) in our spectrum. No such emission feature is seen at the radio position. We also looked for emission in the satellite lines assuming our detection is indeed the 1667 MHz main line at 1058.9 or 1130.0 MHz, with no such features seen. This result is not surprising given the weakness of satellite lines in OHMs (McBride et al. 2013), although as the LADUMA survey proceeds and reaches greater depths, we may be able to detect them in some systems. We also found no evidence of H I emission or absorption at this redshift, although such features may become evident from the upcoming deeper LADUMA observations.

In Figure 3, we consider the implications of WISE magnitudes and colors for our identification of the detected emission line. We employ the algorithms presented in Roberts et al. (2021), who use machine learning to determine the redshift evolution in WISE magnitude and color space for an OHM host and a typical H I source. The predicted distributions in WISE properties expected for gas-rich disk galaxies emitting H I at redshift $z \sim 0.30$ (red) and a galaxy merger traced through OH at redshift $z \sim 0.52$ (blue) show that an OH identification for our source is plausible for all diagnostics, while an H I identification is not always supported (see right

[54] Errors in brackets represent 5% flux scale uncertainties.

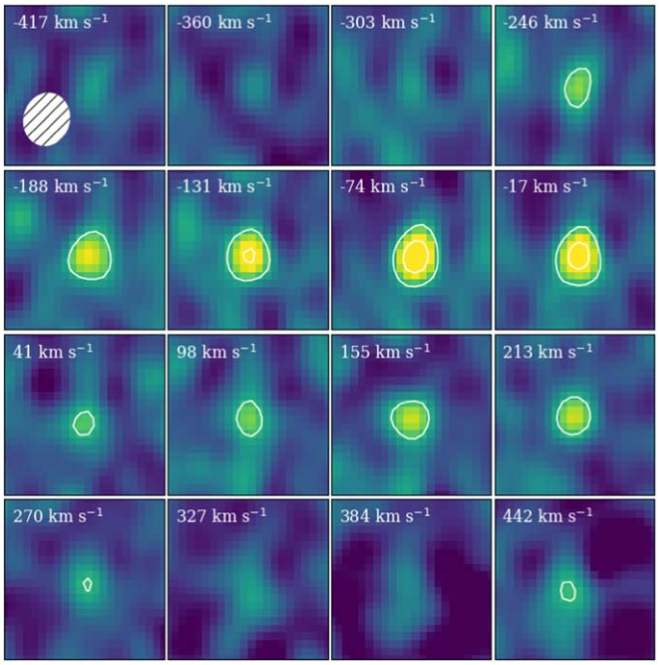

Figure 2. Independent velocity channel maps of an 8× rebinned 26.1 kHz data cube, with velocities indicated relative to our measured systemic redshift of $z_{\rm OH} = 0.5225$. Contours are multiples of 2σ ($1\sigma = 0.283$ mJy beam^{-1}). The $14\farcs2 \times 12\farcs2$ synthesized beam is plotted in the top-left panel.

panel). Therefore, we are confident that the emission detected corresponds to the main OH transition at 1667 MHz.

4. Discussion

4.1. OH and FIR Luminosities

LADUMA J033046.20−275518.1 is one of the most luminous OHMs known at any redshift; only 3 sources within the sample of 53 OHMs presented in Darling & Giovanelli (2002a) and Darling & Giovanelli (2002b) have higher $L_{\rm OH}$ values, and it is only marginally less luminous than the $z = 0.1961$ OHM recently detected by Apertif (Hess et al. 2021), which would have $L_{\rm OH} = 7.18 \times 10^3\, L_\odot$ for our cosmology. In recognition of this power and its unprecedentedly high redshift, we have given it the nickname "Nkalakatha," an isiZulu word that means "big boss." It is not overly surprising that a detection reached in a single LADUMA track will be among the most luminous OHMs when compared to sources from the local universe at $z < 0.27$. Using the relationship between OH and far-IR luminosities derived by Darling & Giovanelli (2002a) for an Arecibo survey + literature sample of OHMs, i.e., $\log(L_{\rm OH}/L_\odot) = (1.57 \pm 0.11) \log(L_{\rm FIR}/L_\odot) - (15.76 \pm 1.22)$, we find that the predicted OH luminosity for LADUMA J033046.20−275518.1 is $L_{\rm OH\ pred} \approx 2.4 \times 10^3\, L_\odot$. This is roughly a factor of 2.6 smaller than what we observe but well within the large scatter observed for the local relation (Figure 4). The dust temperature recovered from the fit to the system's FIR photometry ($T_d \approx 42$ K) is roughly consistent with theoretical expectations and observational results that $T_d \geqslant 45$ K is required for OH masing to occur (Lockett & Elitzur 2008; Willett et al. 2011), particularly if cooler dust outside the masing region contributes to $L_{\rm FIR}$ and is at the lower end of the distribution of global dust temperatures for OHM hosts.

We have also considered the FIR–radio flux ratio parameter q, defined by Helou et al. (1985) as

$$q = \log\left\{\left(\frac{F_{\rm FIR}}{\rm W\ m^{-2}}\right)\left(\frac{10^{29}}{3.75 \times 10^{12}\ \rm Hz}\right)\left(\frac{S_{1.4\ \rm GHz}}{\rm mJy}\right)^{-1}\right\}. \quad (2)$$

For LADUMA J033046.20−275518.1, we correct the observed radio continuum flux density[55] (Table 1) to 1.4 GHz in the rest frame assuming a spectrum $S_\nu \propto \nu^{-0.7}$ and arrive at an estimated $q \approx 2.7$. This value is consistent with the infrared–radio correlation for star-forming galaxies with no evidence of AGNs (see, e.g., Figure 16 of Delhaize et al. 2017), higher than the median $q = 2.37$ recently measured for 89 star-forming galaxies in the COSMOS field (An et al. 2021), and much higher than the threshold $q \approx 1.8$ at which galaxies are three times more radio-loud than the mean for star-forming systems (Condon et al. 2002). Spitzer/IRAC photometry for this source (Lonsdale et al. 2003) also disfavors an AGN identification according to well-established criteria (Stern et al. 2005; Donley et al. 2012), as does a classification of its optical spectrum (Mao et al. 2012). As a result, we view the far-IR emission from LADUMA J033046.20−275518.1 as more likely due to starburst activity than to a bolometrically significant AGN. Such a conclusion is also not surprising given the evidence from the local universe that ULIRGs hosting OHMs are less likely to show evidence of AGNs at infrared wavelengths than nonmasing ULIRGs (Willett et al. 2011).

4.2. A Possible Molecular Outflow

Large-scale outflows emanating from the central regions of galaxies and powered by both starbursts and AGNs have been known for decades to play an important role in the evolution of galaxies and the intergalactic medium (e.g., Heckman et al. 1990). Such outflows have been detected through OH observations in a number of systems. Baan et al. (1989) detect three distinct outflows in emission in a sample of five OHMs, with one galaxy showing a maximum outflow velocity of 800 km s^{-1}. González-Alfonso et al. (2014) meanwhile find far-IR OH features blueshifted by over 1000 km s^{-1} in Mrk 231, with the central AGN likely responsible for the high mass outflow rate and outflow velocities detected.

The OH emission in LADUMA J033046.20−275518.1 is blueshifted by 407 ± 118 km s^{-1} relative to the redshift measured from optical spectroscopy. The simplest explanation for a one-sided velocity offset is a starburst-driven outflow, given the high value of q noted above. However, the situation could be more complex, involving multiple nuclei or a disk close to an (obscured) AGN, possibly interacting with outflows. As our MeerKAT observation of this galaxy and its OH emission is unresolved, higher spatial resolution observations would be required to further characterize the outflow's extent and energetics. The study of Gowardhan et al. (2018), investigating molecular gas outflows in two starburst ULIRGs in mid-J CO and 18 cm OH lines, is instructive in this regard. CO outflow velocities are seen to exceed 1600 km s^{-1}, with corresponding mass outflow rates of 300–700 $M_\odot$ yr^{-1}; meanwhile, OH outflow velocities are seen to extend to

[55] This value is comparable to the value measured from MeerKAT continuum imaging of the LADUMA field, which will be published in a forthcoming paper analogous to Heywood et al. (2022).

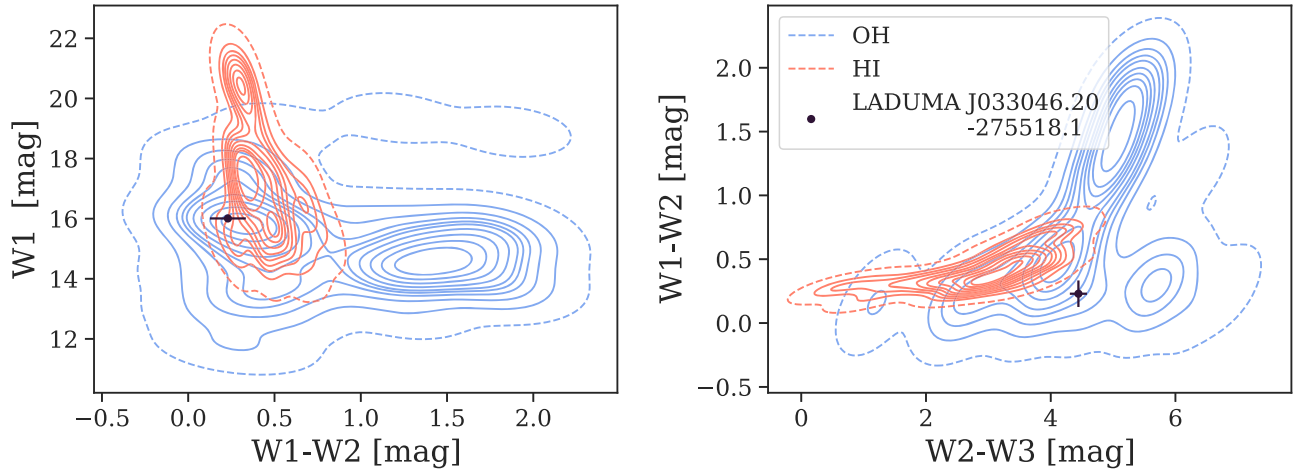

Figure 3. Predicted distributions of gas-rich mergers traced by OH at $z_{\rm OH} \sim 0.52$ (blue), and H I-rich disk galaxies at $z_{\rm H\,I} \sim 0.30$ (red), in WISE color–magnitude and color–color space, generated using algorithms presented in Roberts et al. (2021). Contours enclose the upper 99% (dashed), 90%, 80%,…, 20%, and 10% of the Gaussian kernel density estimates for the respective galaxy distributions. In the left panel, both OH and H I identifications are supported for LADUMA J033046.20 −275518.1, while in the right panel, OH is clearly preferred.

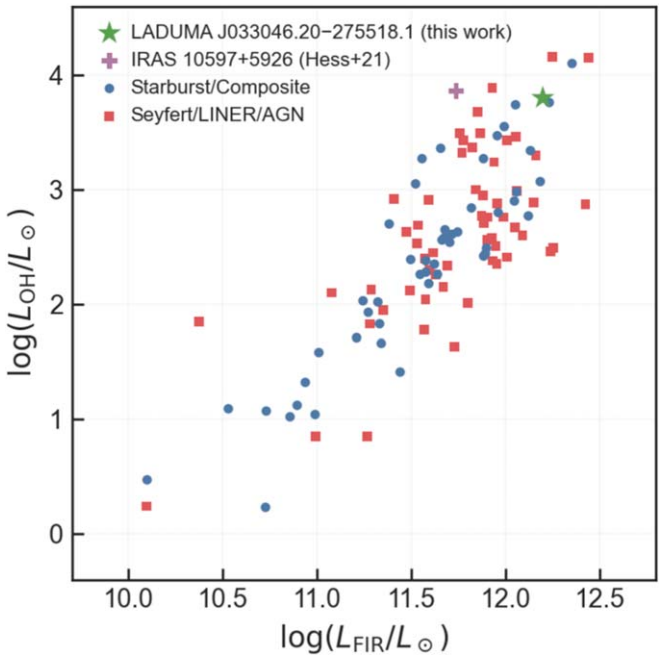

Figure 4. $L_{\rm OH}$ vs. $L_{\rm FIR}$ for known OHMs (H. Roberts et al. 2022, in preparation). LADUMA J033046.20−275518.1 (green star) is one of the most luminous OHMs on both axes.

1000 km s^{-1}, with velocity wings for one source agreeing "remarkably well" with previous detections of outflowing molecular gas. A higher-resolution study of other molecular species (e.g., CO) in LADUMA J033046.20−275518.1 may thus be a productive strategy for confirming the existence of an outflow in OH.

5. Conclusions

We present the first detection of an OHM in the LADUMA field, LADUMA J033046.20−275518.1 "Nkalakatha," which is also the highest-redshift detection of such a system to date in the main 1667 MHz OH emission line. OH emission is found to be redshifted to $z_{\rm OH} = 0.5225$, which agrees well with an optical redshift of $z_{\rm opt} = 0.5246$ for a host galaxy already known to be a ULIRG. The system's total OH luminosity of $L_{\rm OH} = (6.31 \pm 0.18\,[\pm 0.31]) \times 10^3\,L_\odot$ makes it one of the most luminous OHMs known (all other 1667 MHz detections have redshifts $z < 0.27$) and is consistent with its large far-IR luminosity. The $\sim$400 km s^{-1} offset between the OH and optical redshifts is most simply explained by a starburst-driven outflow.

This detection highlights the potential of upcoming spectral line surveys, whose wide frequency coverage will enable further high-redshift measurements. Roberts et al. (2021) predict that 83 ± 20 OHMs will be detected in LADUMA alone, which will nearly double the number of known OHMs. Greater numbers are expected in lower-redshift but wider-area surveys, such as the Widefield ASKAP *L*-band Legacy All-sky Blind surveY (WALLABY; Koribalski et al. 2020), the Apertif Wide-area Extragalactic Survey (AWES; K. M. Hess et al. 2022, in preparation), and the H I component (MIGHTEE-H I; Maddox et al. 2021) of the MeerKAT International GigaHertz Tiered Extragalactic Exploration (MIGHTEE) survey (Jarvis et al. 2016). As LADUMA reaches greater depths, we expect to set further OHM redshift records, which will enable studies of the cosmic rate of gas-rich galaxy mergers and further constrain galaxy evolution models.

The authors sincerely thank Zolile Tibane for suggesting the nickname "Nkalakatha" for LADUMA J033046.20−275518.1. We also thank the anonymous referee for comments that have helped improve the paper.

The MeerKAT telescope is operated by the South African Radio Astronomy Observatory (SARAO; www.sarao.ac.za), which is a facility of the National Research Foundation (NRF), an agency of the Department of Science and Innovation. The authors thank the members of the SARAO engineering, commissioning, and science data processing teams for building and operating an absolutely superb facility. The MeerKAT data presented in this paper were processed using the ilifu cloud computing facility (www.ilifu.ac.za), which is operated by a consortium that includes the University of Cape Town (UCT), the University of the Western Cape, the University of Stellenbosch, Sol Plaatje University, the Cape Peninsula University of Technology and the South African Radio

Astronomy Observatory. The ilifu facility is supported by contributions from the Inter-University Institute for Data Intensive Astronomy (IDIA, which is a partnership between the UCT, the University of Pretoria and the University of the Western Cape), the Computational Biology division at UCT, and the Data Intensive Research Initiative of South Africa (DIRISA). Data processing used pipelines that were developed at IDIA and are available at https://idia-pipelines.github.io.

M.G. acknowledges support from IDIA and was partially supported by the Australian Government through the Australian Research Council's Discovery Projects funding scheme (DP210102103). A.K.M. and A.J.B. acknowledge support from NSF grant AST-1814421. A.K.M. also thanks the LSSTC Data Science Fellowship Program, which is funded by the LSST Corporation, NSF grant OAC-1829740, the Brinson Foundation, and the Moore Foundation; his participation in the program has been helpful for this work. H.R. and Je.D. acknowledge support from NSF grant AST-1814648; M.B. and J.O. acknowledge support from NSF grant AST-1814682; R.B. acknowledges support from an STFC Ernest Rutherford Fellowship (grant No. ST/T003596/1); Ja.D. and H.P. acknowledge the financial assistance of SARAO; K.M.H. acknowledges funding from the State Agency for Research of the Spanish Ministry of Science, Innovation and Universities through the "Center of Excellence Severo Ochoa" awarded to the Instituto de Astrofísica de Andalucía (SEV-2017-0709); from grant RTI2018-096228-B-C31 (Ministry of Science, Innovation and Universities/State Agency for Research/European Regional Development Funds, European Union); and from the coordination of the participation in SKA-SPAIN, funded by the Ministry of Science and innovation (MICIN); and Z.L.H. and S.K. acknowledge support from NSF grant AST-1814486. Parts of this research were supported by the Australian Research Council Centre of Excellence for All Sky Astrophysics in 3 Dimensions (ASTRO 3D), through project number CE170100013, and by the South African Research Chairs Initiative of the Department of Science and Technology and the NRF.

Facility: MeerKAT.

ORCID iDs

Marcin Glowacki https://orcid.org/0000-0002-5067-8894
Jordan D. Collier https://orcid.org/0000-0002-2326-7432
Amir Kazemi-Moridani https://orcid.org/0000-0003-4496-9553
Bradley Frank https://orcid.org/0000-0003-3599-1521
Hayley Roberts https://orcid.org/0000-0003-0046-9848
Jeremy Darling https://orcid.org/0000-0003-2511-2060
Hans-Rainer Klöckner https://orcid.org/0000-0002-0648-2704
Nathan Adams https://orcid.org/0000-0003-4875-6272
Andrew J. Baker https://orcid.org/0000-0002-7892-396X
Matthew Bershady https://orcid.org/0000-0002-3131-4374
Tariq Blecher https://orcid.org/0000-0001-8404-848X
Sarah-Louise Blyth https://orcid.org/0000-0002-5777-0036
Rebecca Bowler https://orcid.org/0000-0003-3917-1678
Barbara Catinella https://orcid.org/0000-0002-7625-562X
Laurent Chemin https://orcid.org/0000-0002-3834-7937
Steven M. Crawford https://orcid.org/0000-0002-8969-5229
Romeel Davé https://orcid.org/0000-0003-2842-9434
Roger Deane https://orcid.org/0000-0003-1027-5043
Erwin de Blok https://orcid.org/0000-0001-8957-4518
Jacinta Delhaize https://orcid.org/0000-0002-6149-0846
Kenneth Duncan https://orcid.org/0000-0001-6889-8388
Ed Elson https://orcid.org/0000-0001-9359-0713
Eric Gawiser https://orcid.org/0000-0003-1530-8713
Julia Healy https://orcid.org/0000-0003-1020-8684
Kelley M. Hess https://orcid.org/0000-0001-9662-9089
Ian Heywood https://orcid.org/0000-0001-6864-5057
Benne W. Holwerda https://orcid.org/0000-0002-4884-6756
Munira Hoosain https://orcid.org/0000-0001-5449-143X
John P. Hughes https://orcid.org/0000-0002-8816-6800
Zackary L. Hutchens https://orcid.org/0000-0002-8574-5495
Matt Jarvis https://orcid.org/0000-0001-7039-9078
Sheila Kannappan https://orcid.org/0000-0002-3378-6551
Neal Katz https://orcid.org/0000-0002-3097-5381
Marie Korsaga https://orcid.org/0000-0002-5882-610X
Renée C. Kraan-Korteweg https://orcid.org/0000-0002-0202-6250
Philip Lah https://orcid.org/0000-0001-6841-6553
Michelle Lochner https://orcid.org/0000-0003-2221-8281
Natasha Maddox https://orcid.org/0000-0001-8312-5260
Sphesihle Makhathini https://orcid.org/0000-0001-9565-9622
Gerhardt R. Meurer https://orcid.org/0000-0002-0163-2507
Martin Meyer https://orcid.org/0000-0002-2838-3010
Danail Obreschkow https://orcid.org/0000-0002-1527-0762
Se-Heon Oh https://orcid.org/0000-0002-8379-0604
Tom Oosterloo https://orcid.org/0000-0002-0616-6971
Joshua Oppor https://orcid.org/0000-0003-2845-2714
Hengxing Pan https://orcid.org/0000-0002-9160-391X
D. J. Pisano https://orcid.org/0000-0001-7996-7860
Swara Ravindranath https://orcid.org/0000-0002-5269-6527
Anja C. Schröder https://orcid.org/0000-0002-2017-584X
Rosalind Skelton https://orcid.org/0000-0001-7393-3336
Oleg Smirnov https://orcid.org/0000-0003-1680-7936
Mathew Smith https://orcid.org/0000-0002-3321-1432
Raghunathan Srianand https://orcid.org/0000-0002-9062-1921
Lister Staveley-Smith https://orcid.org/0000-0002-8057-0294
Masayuki Tanaka https://orcid.org/0000-0002-5011-5178
Mattia Vaccari https://orcid.org/0000-0002-6748-0577
Wim van Driel https://orcid.org/0000-0003-4770-9829
Marc Verheijen https://orcid.org/0000-0001-9022-8081
Fabian Walter https://orcid.org/0000-0003-4793-7880
John F. Wu https://orcid.org/0000-0002-5077-881X
Martin A. Zwaan https://orcid.org/0000-0003-0101-1804

References

An, F., Vaccari, M., Smail, I., et al. 2021, MNRAS, 507, 2643
Baan, W. A., Haschick, A. D., & Henkel, C. 1989, ApJ, 346, 680
Baldry, I. K., Alpaslan, M., Bauer, A. E., et al. 2014, MNRAS, 441, 2440
Blyth, S., Baker, A. J., Holwerda, B., et al. 2016, in Proc. of MeerKAT Science: On the Pathway to the SKA (Trieste: PoS), 4
Briggs, F. H. 1998, A&A, 336, 815
Combes, F., Gupta, N., Muller, S., et al. 2021, A&A, 648, A116
Comrie, A., Wang, K.-S., Ford, P., et al. 2020, CARTA: The Cube Analysis and Rendering Tool for Astronomy, 1.3.0, Zenodo, doi:10.5281/zenodo.3746095
Condon, J. J., Cotton, W. D., & Broderick, J. J. 2002, AJ, 124, 675
Darling, J. 2004, ApJ, 612, 58

Darling, J. 2007, ApJL, 669, L9
Darling, J., & Giovanelli, R. 2002a, AJ, 124, 100
Darling, J., & Giovanelli, R. 2002b, ApJ, 572, 810
DeBoer, D. R., Gough, R. G., Bunton, J. D., et al. 2009, IEEEP, 97, 1507
Dehghan, S., Johnston-Hollitt, M., Franzen, T. M. O., Norris, R. P., & Miller, N. A. 2014, AJ, 148, 75
Delhaize, J., Smolčić, V., Delvecchio, I., et al. 2017, A&A, 602, A4
Donley, J. L., Koekemoer, A. M., Brusa, M., et al. 2012, ApJ, 748, 142
Eales, S., Chapin, E. L., Devlin, M. J., et al. 2009, ApJ, 707, 1779
Franzen, T. M. O., Banfield, J. K., Hales, C. A., et al. 2015, MNRAS, 453, 4020
González-Alfonso, E., Fischer, J., Graciá-Carpio, J., et al. 2014, A&A, 561, A27
Gowardhan, A., Spoon, H., Riechers, D. A., et al. 2018, ApJ, 859, 35
Griffin, M. J., Abergel, A., Abreu, A., et al. 2010, A&A, 518, L3
Hanish, D. J., Capak, P., Teplitz, H. I., et al. 2015, ApJS, 217, 17
Heckman, T. M., Armus, L., & Miley, G. K. 1990, ApJS, 74, 833
Helou, G., Soifer, B. T., & Rowan-Robinson, M. 1985, ApJL, 298, L7
Hess, K. M., Roberts, H., Dénes, H., et al. 2021, A&A, 647, A193
Heywood, I., Jarvis, M. J., Hale, C. L., et al. 2022, MNRAS, 509, 2150
Jarvis, M., Taylor, R., Agudo, I., et al. 2016, in Proceedings of MeerKAT Science: On the Pathway to the SKA (Trieste: PoS), 6
Jarvis, M. J., Bonfield, D. G., Bruce, V. A., et al. 2013, MNRAS, 428, 1281
Jonas, J. & MeerKAT Team 2016, in Proc. of MeerKAT Science: On the Pathway to the SKA (Trieste: PoS), 1
Klöckner, H.-R., Baan, W. A., & Garrett, M. A. 2003, Natur, 421, 821
Koribalski, B. S., Staveley-Smith, L., Westmeier, T., et al. 2020, Ap&SS, 365, 118
Lo, K. Y. 2005, ARA&A, 43, 625
Lockett, P., & Elitzur, M. 2008, ApJ, 677, 985
Lonsdale, C. J., Smith, H. E., Rowan-Robinson, M., et al. 2003, PASP, 115, 897
Maddox, N., Frank, B. S., Ponomareva, A. A., et al. 2021, A&A, 646, A35
Mao, M. Y., Sharp, R., Norris, R. P., et al. 2012, MNRAS, 426, 3334
McBride, J., Heiles, C., & Elitzur, M. 2013, ApJ, 774, 35
McMullin, J. P., Waters, B., Schiebel, D., Young, W., & Golap, K. 2007, in ASP Conf. Ser 376, Astronomical Data Analysis Software and Systems XVI, ed. R. A. Shaw, F. Hill, & D. J. Bell (San Francisco, CA: ASP), 127
Miyazaki, S., Komiyama, Y., Kawanomoto, S., et al. 2018, PASJ, 70, S1
Moncelsi, L., Ade, P. A. R., Chapin, E. L., et al. 2011, ApJ, 727, 83
Oliver, S. J., Bock, J., Altieri, B., et al. 2012, MNRAS, 424, 1614
Perley, R. A., & Butler, B. J. 2017, ApJS, 230, 7
Reddy, N. A., Steidel, C. C., Pettini, M., et al. 2008, ApJS, 175, 48
Reynolds, J. 1994, ATNF Technical Memos, 39.3/040
Rieke, G. H., Young, E. T., Engelbracht, C. W., et al. 2004, ApJS, 154, 25
Roberts, H., Darling, J., & Baker, A. J. 2021, ApJ, 911, 38
Shirley, R., Duncan, K., Campos Varillas, M. C., et al. 2021, MNRAS, 507, 129
Stern, D., Eisenhardt, P., Gorjian, V., et al. 2005, ApJ, 631, 163
Suess, K. A., Darling, J., Haynes, M. P., & Giovanelli, R. 2016, MNRAS, 459, 220
Takeuchi, T. T., Buat, V., & Burgarella, D. 2005, A&A, 440, L17
Willett, K. W., Darling, J., Spoon, H. W. W., Charmandaris, V., & Armus, L. 2011, ApJ, 730, 56
Wong, K. C., Suyu, S. H., Chen, G. C. F., et al. 2020, MNRAS, 498, 1420
Wright, E. L., Eisenhardt, P. R. M., Mainzer, A. K., et al. 2010, AJ, 140, 1868